



## **JRA-1 Milestone: Validation of the Final Sensor Equipping the EUDET Beam Telescope.**

J. Baudot \*, G. Bertolone\*, G. Claus\*, C. Colledani\*, Y. Degerli†, R. De Masi\*, A. Dorokhov\*,  
G. Dozière\*, W. Dulinski\*, M. Gelin†, M. Goffe\*, F. Guilloux†, A. Himmi\*, Ch. Hu-Guo\*,  
K. Jaaskelainen\*, F. Morel\*, F. Orsini†, M. Specht\*, I. Valin\* and M. Winter\*

August 31, 2009

### **Abstract**

The final sensor developed for the EUDET beam telescope has been fabricated and successfully tested during the last year. The sensor performances were assessed in the laboratory and by running simultaneously up to 6 sensors on a minimum ionising particle beam at the CERN SPS. The results obtained validate the sensors fully for their use in the telescope.

More information on the topics described in this document may be found on the web site of IPHC:  
<http://www.iphc.cnrs.fr/Cmos.html>

---

\*IPHC/IReS, CNRS/IN2P3, ULP/UdS, 23 rue du loess, BP28, 67037 Strasbourg cedex 2, France

†IRFU, CEA - Saclay, 91191 Gif sur Yvette Cedex, France

# 1 Overview of the sensor development

To achieve the pixel sensor required for the EUDET beam telescope (BT), an integrated micro-circuit architecture was developed, where the signals delivered by the sensors are discriminated before being filtered by an integrated zero-suppression logic. The fast read-out ambitionned was achieved by grouping the pixels composing the sensitive area in columns read out in parallel.

The development of this sensor was addressed through two parallel tasks. One of them encompassed the upstream part of the signal conditioning chain, ranging from the pixel array to the discriminators ending the columns. The other concerned the downstream part, combining a zero-suppression logic with output memories and the data transmission circuitry.

Small prototypes were fabricated and tested in previous years to develop the upstream part of the sensor architecture. IDC (alias *MIMOSA-22*) is the final prototype of this R&D line. Its performances, summarised in a former EUDET report [1], validated the pixel and column parallel architectures.

The zero-suppression micro-circuitry and the output memories composing the downstream part of the sensor architecture were prototyped with the chip called SDC-2 (alias *SUZE*). Fabricated in 2007, it was validated in 2008 at frequencies well above the nominal value [2].

This outcome of IDC and SDC-2 allowed to move to the design and fabrication of the final - full scale - sensor, called TC (alias *MIMOSA-26*), which was designed in 2008 and came back from foundry early in 2009.

## 2 Description of the sensor

The sensor combines the designs of the IDC and SDC-2 chips, and extends them from 128 to 1152 columns, each ended with a discriminator. Each column contains 576 pixels featuring a pitch of  $18.4 \mu\text{m}$ . The total number of pixels composing the sensor ( $\sim 660\,000$ ) allows to cover a sensitive area of  $\sim 21.2 \times 10.6 \text{ mm}^2$ .

Figure 1 displays the block diagram of the sensor. The rolling shutter mode is steered through a row selector & pixel sequencer located on the left side. The voltage signal induced by the charges collected is amplified in each pixel by a preamplification stage. The information from two successive frames is subtracted by the clamping technique in order to perform the CDS. The 1152 pixel signals of the selected row are transmitted to the bottom of the pixel array where 1152 column-level, offset compensated discriminators ensure the analogue-to-digital conversion. A second double sampling, implemented in each discriminator stage, removes pixel to pixel offsets introduced by each in-pixel buffer [3]. This allows using a common threshold for all discriminators.

Their outputs are connected to a zero-suppression circuitry, organised in a pipeline mode, which scans the sparse data of the current row. This is achieved in two consecutive steps. The one closest to the discriminator outputs is split into 18 blocks of 64 columns. Inside

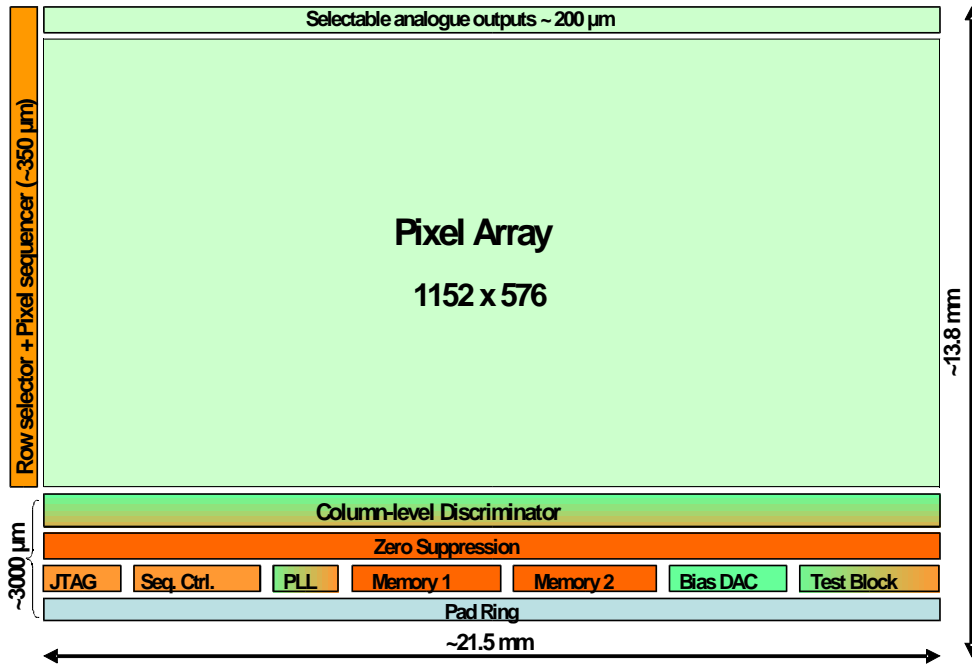


Figure 1: Block-diagram of the TC sensor. The uniform green surface stands for the sensitive area. The signal processing circuitry is integrated at the chip periphery visible at the bottom, complemented with a narrow,  $< 400 \mu m$  wide, vertical band visible on the left, used for the row by row addressing. A  $\sim 200 \mu m$  wide band along the top of the picture contains the circuitry achieving the (slow) read-out of the pixels for their individual functionality tests.

each block, the circuitry scans the 64 columns, skipping non-hit pixels and identifying contiguous pixels (building a so-called "string") having their signals above the threshold. It considers up to 6 strings per block, each string being composed of up to 4 hit pixels. In the second stage, the outputs of the 18 blocks are combined in up to 9 strings, strings overlapping two neighbouring blocks being merged in a single one. The length and addresses of the string's beginning are stored in one of the two SRAMs, thus allowing a continuous read-out (while one SRAM is being filled, the other is being read out).

A data compression factor ranging from 10 to 1000 can be obtained, depending on the hit density per frame. The collection of sparsified data belonging to a frame is then sent out during the acquisition of the next frame via one or two 100 Mbits/s LVDS transmitters.

An optional Phase-Locked Loop (PLL<sup>1</sup>) module is allowing a high frequency clock generation based on a low frequency reference input block.

The on-chip programmable biases, voltage references and the selection of the test mode are set via a JTAG controller. The sensor incorporates the possibility to test each logical block (pixels, discriminators, zero-suppression circuitry and data transmission).

### 3 TC fabrication yield

6 wafers were fabricated, each composed of 77 sensors. 41 sensors were diced out of 1 unthinned wafer and 1 full wafer was thinned to 120  $\mu m$  and completely diced. Up to now, 21 unthinned and 6 thinned sensors were mounted on an interface board and characterised. Figure 2 shows a photograph of one of the sensors mounted on its interface board.

The sensors functionality tests revealed the following yield related results :

- 23 sensors were found fully operational
- 1 sensor was found unusable
- 1 sensor was found with 1 dead row and 1 dead column (i.e. 0.26 % dead pixels)
- 2 sensors were found with either 1 dead column (i.e. 0.09 % dead pixels) or 1 dead row (0.17 % dead pixels)

Since sensors featuring 1 dead row or column can still be considered as valid, the fabrication yield can be estimated to  $\gtrsim 90$  %.

The sensors were tested extensively in the laboratory. The tests were first performed with the analog part in order to check the pixel response over the complete sensitive area. Next the digital outputs were tested, in 4 different configurations:

- 1152 discriminators alone (isolated from the pixel array)

---

<sup>1</sup>A PLL block is a feedback control system that automatically adjusts the phase of a locally generated signal to match the phase of an input signal.

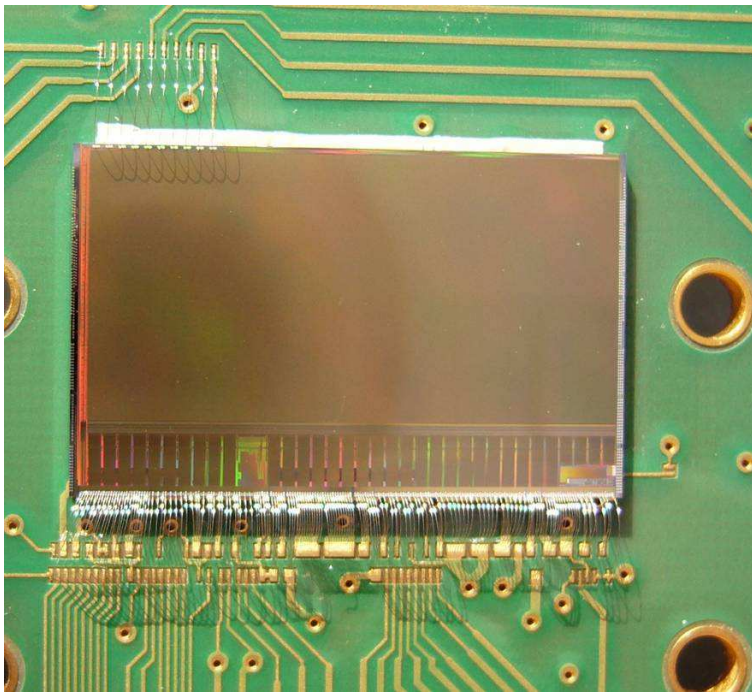


Figure 2: Photograph of a TC sensor mounted on an interface board.

- all discriminators connected to the pixel array
- zero-suppression circuitry alone
- full chain including the pixel array, the discriminators and the zero-suppression logic.

The chip operation was started with a slightly slower read-out than the one of IDC, because of the large number of discriminators (1152) working in parallel. The initial frame read-out frequency was set to  $\sim 9\,000$  frames per second. It will be increased progressively, once it will have been checked that the discriminators stay all well synchronised and provide a well controlled uniform threshold value. The ultimate operation speed will thus be reached after the sensor commissioning.

The sensors are still being tested. Some of the main results obtained up to now are summarised in this sub-section.

## 4 TC characterisation in the laboratory

### 4.1 Tests of the analog part of the sensor

The analogue response was studied on 8 different sensors in order to evaluate the pixel noise, the charge collection efficiency and the uniformity of the response over the sensitive area. All sensors exhibited very similar performances.

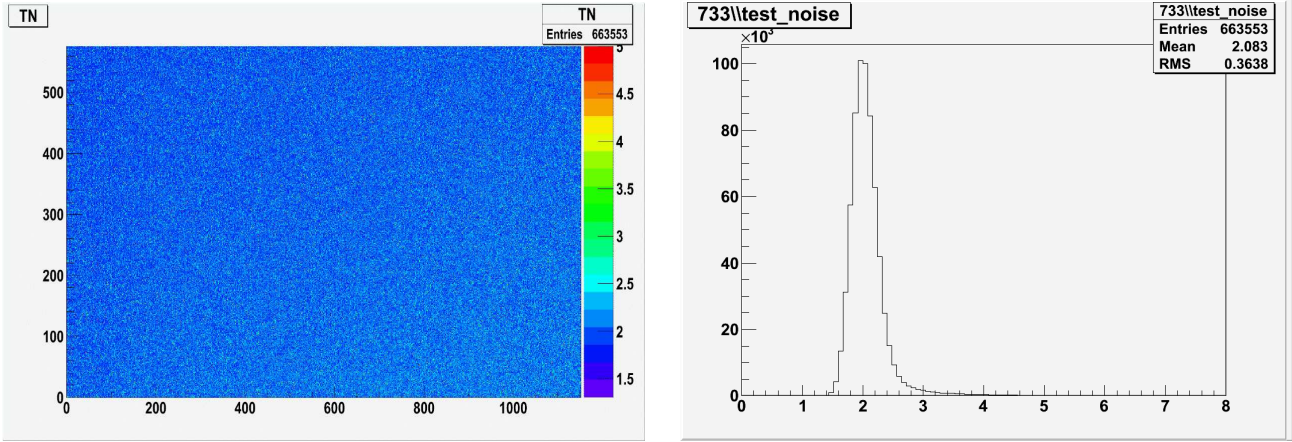


Figure 3: TC pixel noise distribution at the nominal frequency (80 MHz). The noise is shown for each pixel composing the sensitive area on the left. The distribution of the noise of all pixels is displayed on the right in ADC units (1 ADC  $\simeq$  6.5 e<sup>-</sup>).

The result of the pixel noise measurements is illustrated by Figure 3, which displays the noise value of all pixels composing one of the sensors. One observes that the noise is uniformly distributed ( $\sim$  15 % dispersion around the mean value) and that there are no dead pixels. The average noise value amounts to  $\lesssim$  14 e<sup>-</sup>ENC at a read-out frequency of 80 MHz. It decreases to  $\lesssim$  12 e<sup>-</sup>ENC at 20 MHz.

The charge collection efficiency (CCE) was investigated by illuminating the sensors with an <sup>55</sup>Fe source. The CCE was derived from the reconstructed clusters generated by the 5.9 and 6.49 keV X-Rays. The measured values are shown in Table 1, where they are compared to the CCE values observed with IDC. The latter are well reproduced with TC<sup>2</sup>, which validates the extension of the IDC pixel design at full scale.

Cluster size	seed	2x2	3x3	5x5
TC	22 %	55 %	73 %	83 %
IDC	22 %	58 %	75 %	86 %

Table 1: TC CCE measurements compared to those of IDC, when illuminated with an <sup>55</sup>Fe source. The fraction of the cluster charge collected is displayed for the seed pixel (defined as the pixel having collected the largest charge in a cluster) and for clusters composed of 2×2, 3×3 and 5×5 pixels.

<sup>2</sup>The residual differences are compatible with sensor to sensor variations.

## 4.2 Tests of the digital part

The behaviour of the discriminators isolated from the pixel array was studied on 15 unthinned and 6 thinned sensors. The steering of the discriminators being organised in 4 groups, each addressing 288 contiguous columns, the noise performance was estimated for each group separately. The measurement consisted in estimating the response of the discriminators to a fixed voltage by raising progressively their threshold.

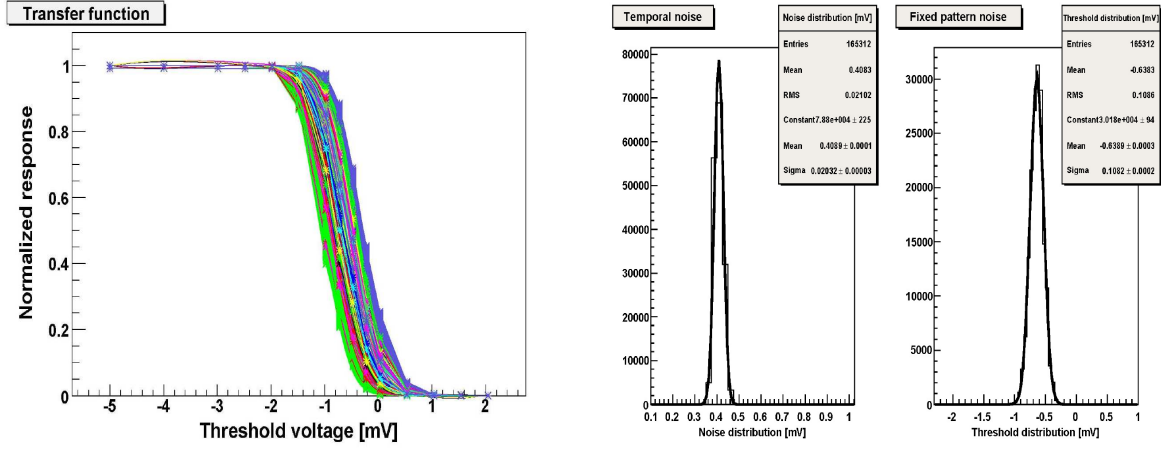


Figure 4: Response of a group of 288 isolated discriminators composing a TC sensor to an external voltage injected upstream of the discriminators, as a function of the threshold value. The threshold scan is shown on the left, while its interpretation in terms of thermal and fixed pattern noises is shown, respectively, in the middle and on the right of the figure.

The outcome of the study is illustrated in Figure 4, which displays the response of a group of 288 discriminators as a function of the threshold value. One observes that all discriminators fire at low threshold and that a transition towards no firing occurs for voltages above -2 mV. The slope of the transition and its dispersion were interpreted in terms of Temporal (TN) and Fixed Pattern Noise (FPN). The latter are shown in the middle and the right hand side of the figure. The TN amounts to  $\sim 0.4$  mV while the FPN is only  $\sim 0.2$  mV, a modest value when compared to the pixel noise, which exceeds 0.5 mV. These results reproduce well the observations made with IDC, and show that all discriminators are fully operational at nominal read-out frequency.

Next the discriminators were connected to the pixel array. The chip response was assessed at 80 MHz ( $112.5 \mu\text{s}$  frame read-out time) with the 15+6 sensors mentioned earlier. 4 sensors were also studied at a read-out frequency of 20 MHz. The noise measurements performed with isolated discriminators were repeated with each group of 288 connected discriminators. The values observed are shown for one group in Figure 5.

The total TN amounts to  $\sim 0.6$ – $0.7$  mV, which is basically the value of the pixel TN. The total FPN amounts to  $\sim 0.2$ – $0.3$  mV, which is dominated by the discriminator contribution. These values remain nearly constant when varying the read-out frequency

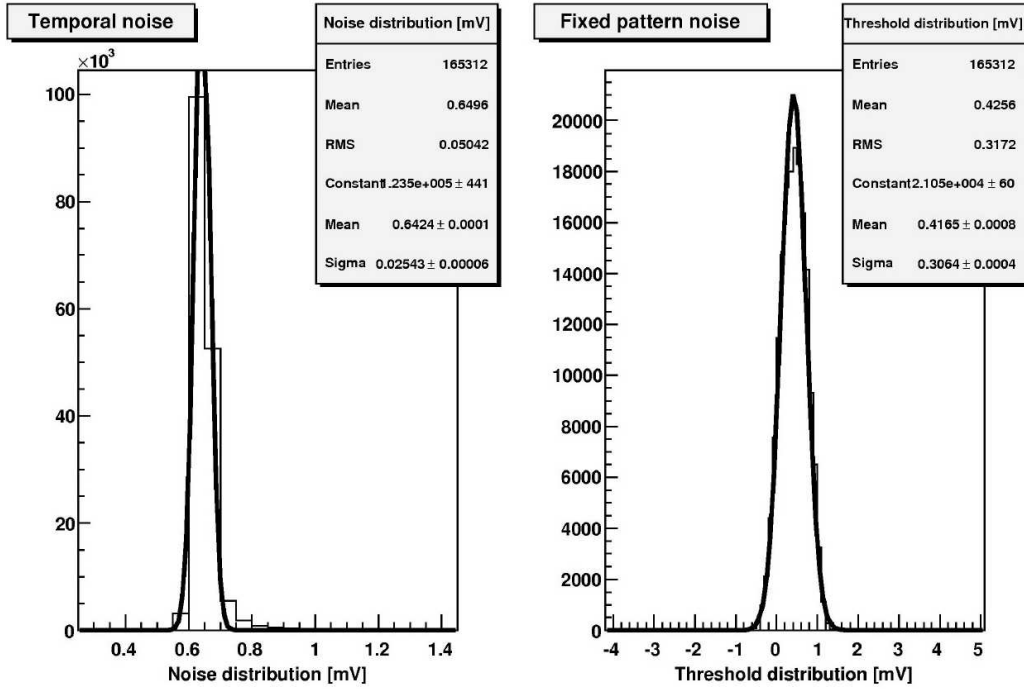


Figure 5: Response of a group of 288 discriminators connected to the pixel array composing a TC sensor. The TN (left) and the FPN (right) distributions were derived from a threshold scan similar to the one at the origin of Figure 4.

from 80 to 20 MHz. The conclusion of the tests at this stage is that the complete array reproduces the performances extrapolated from the IDC prototype [1].

Next, the zero-suppression logic was investigated, disconnected from the rest of the chip. Various patterns were emulated with a pattern generator, and ran through the logic millions of times without any error up to frequencies of 115 MHz (i.e. 1.15 times the nominal frequency). All critical configurations, e.g. with strings overlapping two contiguous blocks, were checked repeatedly to be treated properly.

Finally, the signal processing of the complete chain, ranging from the pixel array to the output of the zero-suppression logic, was characterised on several different sensors. Their output was studied in absence of any radiation source in order to evaluate the fake hit rate due to noise fluctuations as a function of the discriminator threshold. Table 2 summarises the results.

<b>Discriminator threshold</b>	4 N	5 N	5.5 N	6 N	8 N	10 N
$N_{pix} > \text{threshold} (10^{-4})$	$\lesssim 8$	$\sim 1.5$	$\sim 1$	0.5	0.1	0.03

Table 2: Fake hit rate of a TC sensor measured as a function of the discriminator thresholds, in absence of radiation source (noise run).

One observes that discriminator threshold values ranging from 5 to 5.5 times the noise value allow maintaining the fake hit rate at a level of  $10^{-4}$  (i.e.  $< 1$  pixels per frame). This result remains essentially unchanged when varying the operation temperature from  $+20^{\circ}\text{C}$  to  $+40^{\circ}\text{C}$ . It was also checked that multi-hit frames translate into the right output memory patterns.

Finally, the power consumption of the sensor was measured. The static contribution is in the order of 600 mW, i.e.  $\lesssim 300 \text{ mW/cm}^2$ . This value compares well to the consumption estimated per column, of  $\sim 500 \mu\text{W}$ . The latter value is almost equally distributed between the pixels ( $\sim 200 \mu\text{W}$ ) and the discriminators ( $\lesssim 300 \mu\text{W}$ ). The total dynamic power consumption was estimated to be in the order of 200 mW for an occupancy of  $\sim 1\%$ .

## 5 Beam test results

From July 2009, TC was operated 3 times on particle beams at the CERN-SPS. Part of these beam periods were devoted to the integration of the sensors in the EUDET beam telescope, some other ones were performed to evaluate the sensor performances.

The tests started with a set of 3 sensors introduced as Device Under Test (DUT) in the EUDET telescope demonstrator. The 3 sensors were operated synchronously and the track reconstruction was running smoothly after only a few days of run. The next step of the EUDET programme consisted in replacing all 6 analog output sensors composing the telescope demonstrator with TC chips, which are  $> 10$  times faster and 4 times larger. The complete telescope was finally commissioned with  $\gtrsim 100 \text{ GeV}$  pions at the CERN-SPS.

6 other sensors, some of them thinned to  $120\ \mu\text{m}$ , were combined to build another telescope, which was installed at the CERN-SPS for the sensor assessment. They were operated during about 10 days with  $\gtrsim 100\ \text{GeV}$  pions and their response to the beam particles were studied as a function of the discriminator threshold value.

## 5.1 Noise and fake hit rate

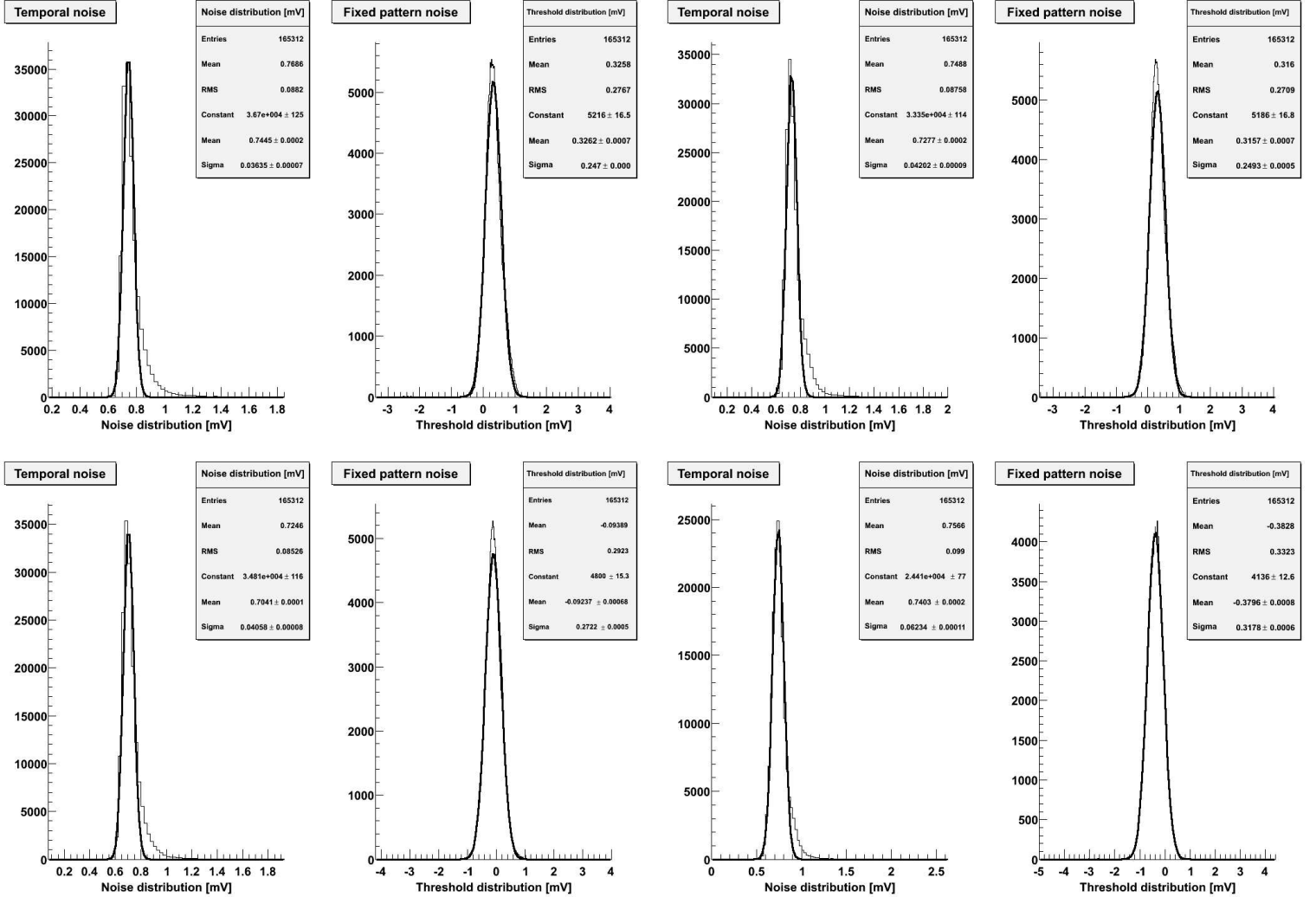


Figure 6: Preliminary TC beam test results: distributions of the TN and FPN measured for each group (called A, B, C, D) of 288 columns at 80 MHz.

A discriminator threshold scan was performed, similar to those performed in the laboratory (see sub-section 4.2), in order to first derive the value of the total noise. The TN and FPN values obtained at a read-out frequency of 80 MHz for the 4 different groups of columns of one of the sensors are displayed in Figure 6. Depending on the sensor,

the TN was found to be  $\sim 0.6\text{-}0.7$  mV and the FPN was observed to be  $\sim 0.3\text{-}0.4$  mV. These values reproduce well those observed in the laboratory (see sub-section 4.2). Next, the rate of fake hits was determined (at room temperature). Table 3 summarises the results for two different sensors, illustrating the spread of the responses between chips. One observes that a threshold slightly above 5 times the noise value allows to keep the fake hit rate in the ordre of  $10^{-4}$  or below, translating typically into 40–80 pixels firing the read-out circuitry per frame.

<b>Discriminator threshold</b>	5 N	6 N	7 N	8 N	10 N	12 N
<b>Fake rate of chip Nr. 24 (<math>10^{-4}</math>)</b>	1.6	0.6	0.24	0.095	0.026	0.017
<b>Fake rate of chip Nr. 1 (<math>10^{-4}</math>)</b>	3.3	1.2	–	0.23	0.054	–

Table 3: Preliminary TC beam test results: values of the average fake hit rate due to pixel noise fluctuations as a function of the discriminator threshold at 80 MHz. The latter are expressed in units of the SNR. The fake rate is indicated in  $10^{-4}$  units for two different sensors.

The characteristics of the noise of the pixel array were studied in some detail in ordre to evaluate its impact on the occupancy of the zero-suppression logic. Figure 7 illustrates the situation observed with chip Nr.1 (mentioned in Table 3) in case of a threshold equivalent to 6 times the noise value. The left side of the figure shows the distribution of the number of hits per frame above threshold observed while collecting 40,000 frames. One observes that the average value of fired pixels per frame is about 80. Compared to the total number of pixels composing the sensor ( $\sim 660,000$ ), this corresponds to a rate of  $\sim 1.2 \cdot 10^{-4}$ . The noise fluctuations above the threshold follow a gaussian (more precisely a Poisson) distribution, with a standard deviation equal to the square root of the mean value.

The right hand side of the figure allows to understand whether the noise fluctuations are rather concentrated in a few pixels firing frequently or if they are more distributed among a large number of pixels firing from time to time. The horizontal axis represents the range covered by the number of times individual pixels generate a fluctuation above threshold within 40,000 frames. This number is actually displayed normalised to the number of frames in ordre to correspond to the fake rate. The vertical axis expresses the number of pixels having fired a given number of times. This number is shown normalised to the total number of pixels. One observes that the majority of the pixels generates noise fluctuations above threshold at a rate ( $O(10^{-5})$ ) well below the average value ( $\sim 10^{-4}$ ), and that a relatively modest fraction of the pixels generates most of the fake hits. For instance, a few per-mill of the pixels fire at least once every 100 frames due to their noise fluctuation. More statistics is needed to evaluate how these values compare from one sensor to another.

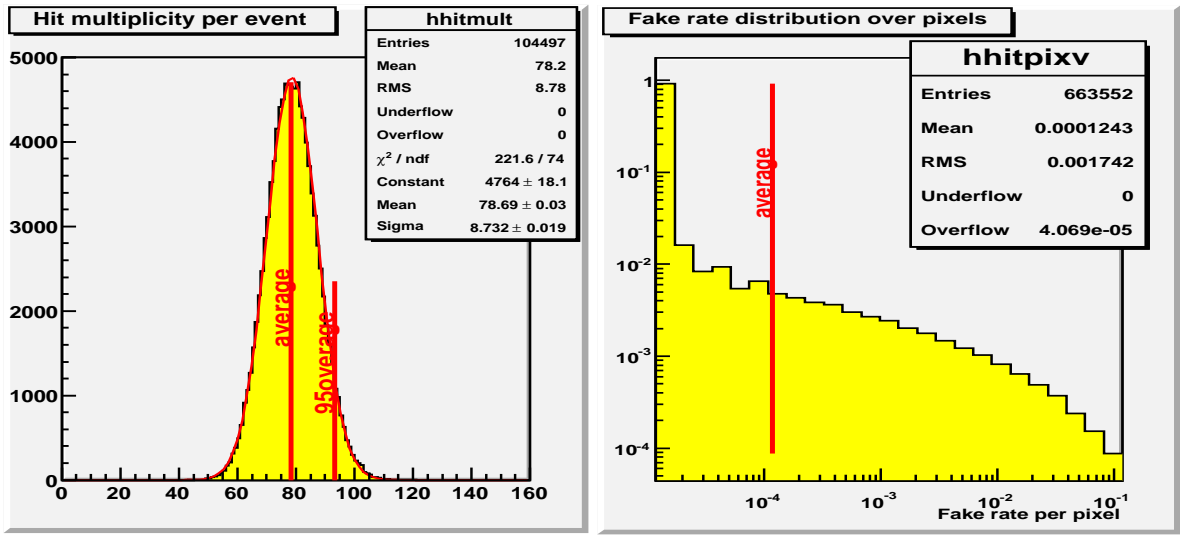


Figure 7: Preliminary TC beam test results based on a sample of  $\sim 40,000$  frames. Left: number of pixels per frame (i.e. fake hit rate) with a noise fluctuation passing a discriminator threshold of  $6N$ . Right: distribution of the fake rate per pixel, normalised to the total number of pixels. The horizontal axis corresponds to the fraction of frames where the noise fluctuations of a pixel are in excess of the threshold value.

## 5.2 Detection efficiency

The detection efficiency was evaluated next for different threshold values and on different sensors, together with the cluster multiplicity distribution and the single point resolution. The events collected were triggered with a  $7 \times 7 \text{ mm}^2$  scintillator slab. Good quality tracks were reconstructed through the telescope for  $\sim 80 \%$  of the triggers. Figure 8 shows the distribution of the particles' impacts in each of the 6 sensors, providing an image of the beam spot based on about 10,000 reconstructed tracks. The correlation between the impacts in different planes is clearly visible.

A detection efficiency of  $\sim 99.5 \pm 0.1\%$  was achieved for a fake rate of  $\sim 10^{-4}$  (see Figure 9). This very satisfactory performance is however slightly below the one observed with IDC. Besides the preliminary aspect of the analysis, which may be partly at the origin of the difference, the latter is also suspected to follow from the large number (1152) of discriminators integrated in TC, translating into threshold dispersions which are slightly limiting the sensor performance. Solutions to this feature exist, which will be implemented in the next generation of sensors.

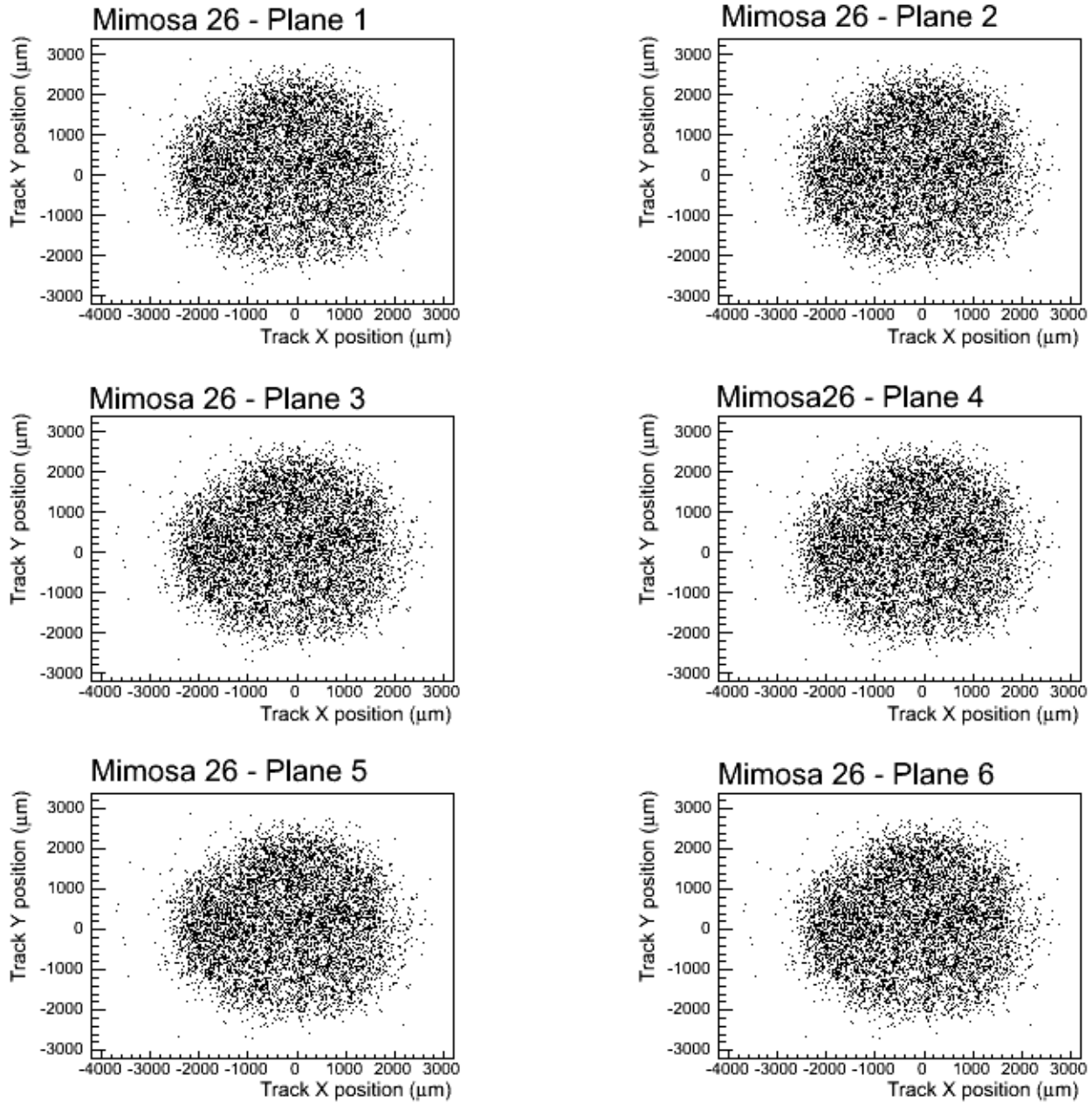
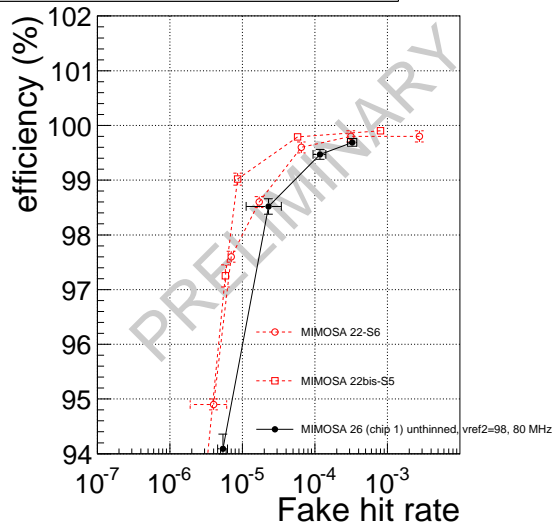


Figure 8: TC beam tests: beam spot derived from about  $10^4$  beam particle tracks reconstructed through the 6 planes of the telescope.

**Efficiency vs Fake hit rate**



**Fake hit rate vs Threshold**

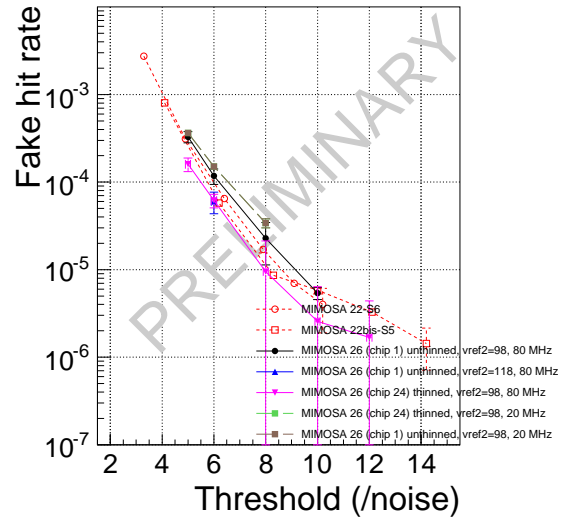
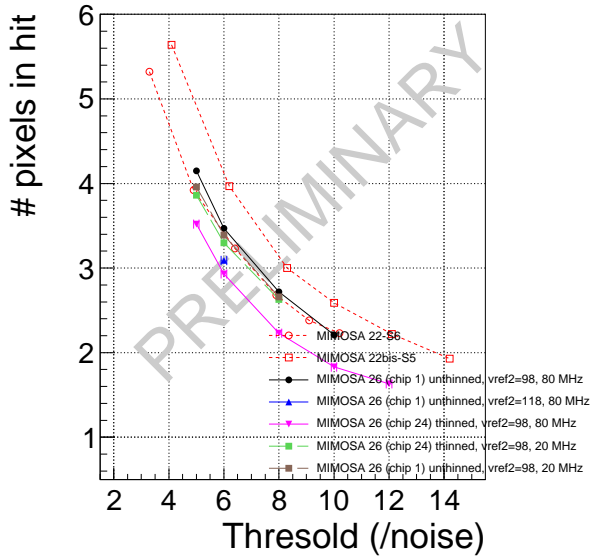


Figure 9: Preliminary TC beam test results: variation of the detection efficiency with the fake hit rate (left), compared to IDC, and threshold dependence of the fake hit rate (right). The threshold values are provided as multiples of the noise value (N).

**Pixel multiplicity vs Threshold**



**Pixel multiplicity in cluster**

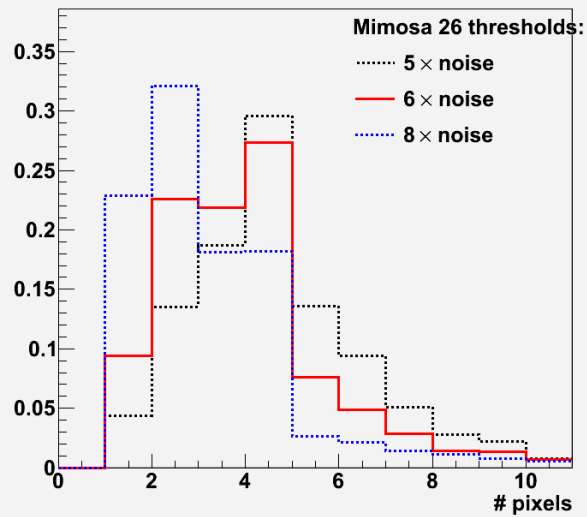


Figure 10: Preliminary TC beam test results: average signal cluster multiplicity as a function of the discriminator threshold varied from 3 to 14 times the noise value (left), and multiplicity distribution for three values of this threshold (right), corresponding to 5, 6 and 8 times the noise value.

### 5.3 Cluster characteristics and single point resolution

Finally, the threshold dependence of the cluster multiplicity and of the single point resolution were evaluated. Figure 10 displays the cluster multiplicity for 3 different threshold values, as well as its average as a function of the threshold. The average cluster multiplicity concentrates around a value of 4 (resp. 3.5) pixels hit for a discriminator threshold corresponding to 5N (resp. 6N), as already observed with IIDC. The dispersion between different sensors is well explained by chip to chip variations observed previously within the same batch. The cluster multiplicity distribution shows that a significant fraction of the signal clusters (e.g.  $\sim 5\%$  for a threshold of 5N) are made of only 1 pixel. Isolated pixels, which are mainly due to pixel noise fluctuations, can therefore not be rejected in order to reduce the fake hit rate.

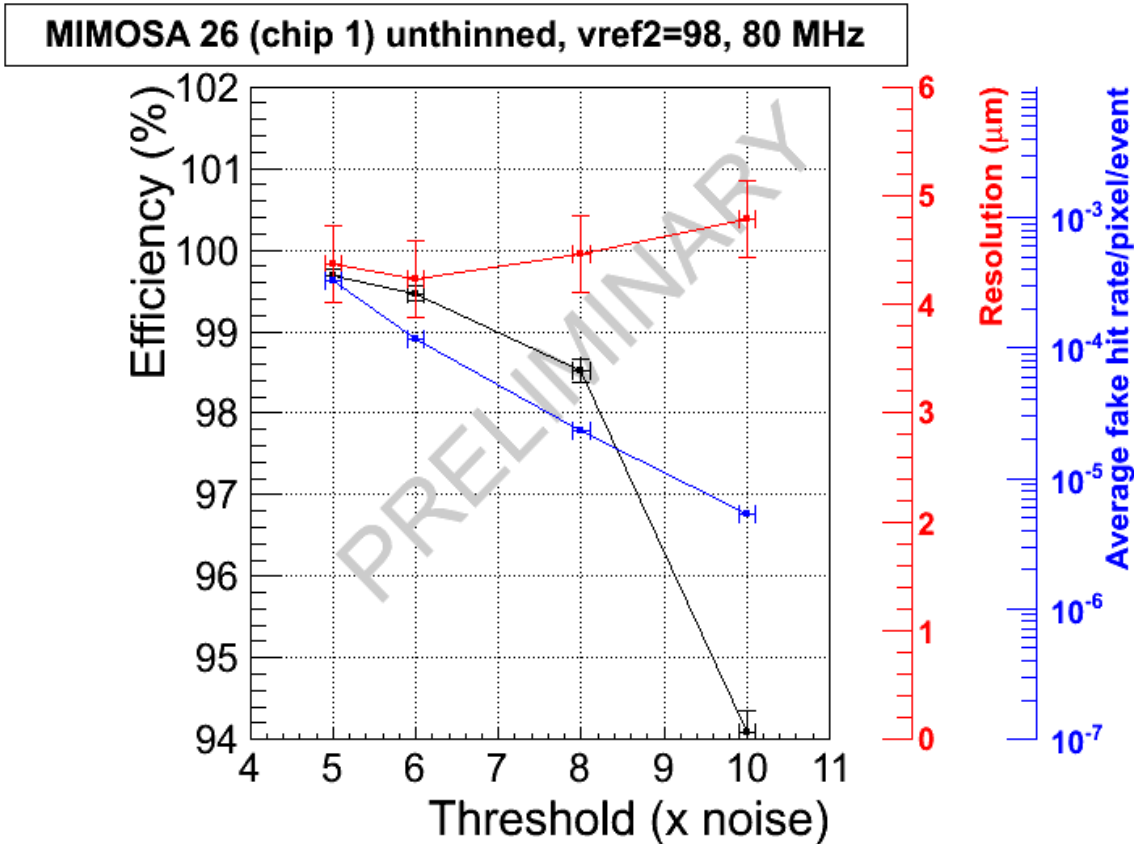


Figure 11: TC preliminary beam test results: variations of the detection efficiency (in black), of the fake hit rate (in blue) and of the single point resolution (in red) with the discriminator threshold value (expressed as multiples of the sensor noise).

Figure 11 displays the variation of the measured resolution with the discriminator threshold. Its value varies between 4 and 4.5  $\mu\text{m}$ , which exceeds the values observed with IDC by  $\gtrsim 0.5 \mu\text{m}$ . This feature is not consistent with the observed cluster characteristics

of TC, which can be considered as indential to those of IDC. This slight inconsistency is being investigated

The figure summarises also the variation of the detection efficiency and of the fake hit rate, and provides therefore an overview of the three main parametres dictating which operation threshold should be retained. A typical threshold value around 5.5N provides clearly satisfactory performances.

The assessment of TC is not yet fully achieved but the evidence is already there that the sensor provides the performances needed for the EUDET beam telescope.

## 6 Summary and conclusion

The final sensor, called TC, developed to equip the two arms of the EUDET beam telescope was designed, fabricated and characterised. The sensor features  $\sim 665\,000$  pixels grouped in 1152 columns, each ended with a discriminator. The column (binary) outputs are processed through a zero-suppression circuitry integrated on the chip periphery. The sensors are read out at a frequency close to  $10^4$  frames/s, and allow to treat several millions of hits per second.

Several sensors were exposed to a high energy particle beam. A detection efficiency of nearly 100 % was obtained for signal discrimination thresholds allowing to keep the fake hit rate in the ordre of  $10^{-4}$  or below. A single point resolution of  $\lesssim 4.5 \pm 0.2 \mu\text{m}$  was observed, translating into a resolution on the impact positions at the DUT surface of  $\sim 2 \mu\text{m}$ .

The sensors were also operated in a beam telescope configuration where 6 devices were running simultaneously at nominal speed. This final test demonstrated that the TC pixel sensors are indeed ready to be used in the EUDET telescope.

## 7 Acknowledgement

This work is supported by the Commission of the European Communities under the 6th Framework Programme "Structuring the European Research Area", contract number RII3-026126.

## References

- [1] G. Claus et al., *IDC, alias MIMOSA-22, status report* EUDET-Memo-2008-03;
- [2] A. Himmi et al., *SDC-2, alias SUZE, zero suppression micro-circuit status report*, EUDET-Memo-2007-55;
- [3] Y.Degerli et al., *Development of Binary Readout CMOS Monolithic Sensors for MIP Tracking*, *IEEE Trans. Nucl. Sci.* 56 (2009) 354.